Proc. of the European Safety and Reliability Conference (ESREL 2026)
Edited by José C. Matos, Paulo B. Lourenço, Michael Beer, Daniel Oliveira, Edoardo Patelli, Hélder S. Sousa, Rui A. Silva and Monica Santamaria

doi: 10.3850/ESREL2026061419_esrel26-p28971-cd

Explainable Fault Diagnosis Driven by Maintenance Expenditure in Power Systems

Ruoran Han

Beihang University[1], Beijing Huairou Laboratory[2], China. E-mail: hanruoran@buaa.edu.cn

Jie Liu*

Beihang University[1], Beijing Huairou Laboratory[2], China. E-mail: liujie_rse@buaa.edu.cn

Abstracts To improve the economic performance and operational reliability of wind-powered integrated energy systems, this paper proposes an explainable fault diagnosis framework. It explicitly embeds maintenance expenditures into the training objective of diagnostic models. Specifically, a cost-sensitive fault diagnosis method is developed based on the Economic Manufacturing Quantity (EMQ) model. Conventional “estimate-then-optimize” approaches prioritize diagnostic and prognostic accuracy while overlooking economic consequences, may resulting in suboptimal maintenance decisions under model misspecification. To bridge this gap, we present an integrated “estimation-and-optimization” strategy that embeds a maintenance cost model into the learning objective. A neural-network-based diagnostic model is trained to minimize both the expected maintenance cost (derived from the EMQ-based production–inventory–maintenance formulation) and a standard statistical loss, thereby aligning prediction targets with decision-making goals. A case study demonstrates that the proposed approach reduces maintenance-related expenditures and improves decision stability while preserving comparable diagnostic accuracy. The results highlight the practical value of cost awareness and explainable diagnosis for enhancing the economic efficiency of prognostics and health management frameworks in modern power and energy systems.

Keywords: Fault Diagnosis, Economic Manufacturing Quantity, Maintenance.

1. General Appearance

With the accelerating integration of large-scale renewable generation, wind-to-hydrogen and its downstream coupling with hydrogen storage and hydrogen loads have attracted increasing attention. A wind–hydrogen production–hydrogen storage integrated system can (i) improve wind power utilization and (ii) provide flexible, low-carbon energy carriers for power systems. However, such systems typically involve multiple tightly coupled subsystems, complex production processes, and non-negligible degradation dynamics, which jointly increase operational and maintenance complexity.

Most fault diagnosis studies emphasize diagnostic accuracy, while comparatively fewer works integrate the *economic consequences* of post-diagnosis maintenance outcomes—such as the cost impact of false alarms and missed detections—into a unified optimization framework. This limitation weakens the interpretability of the model’s optimization direction from a decision-making perspective. For example, Zhang et al. proposed a deconfounding-enhanced image-based knowledge distillation framework to improve fault identification in manufacturing processes [1]; Zheng et al. fine-tuned pre-trained large language models and evaluated their diagnostic accuracy on fault diagnosis tasks in complex systems [2]; and Zheng et al. further incorporated causal paths to develop a hierarchical graph convolutional attention network, thereby enhancing fault detection performance in complex mechatronic systems [3].For wind–hydrogen–storage systems, the consequences of different fault types and diagnostic outcomes can vary dramatically. For example, a false alarm on a minor sensor fault may only trigger a small preventive-maintenance expense. In contrast, an undetected severe electrolyzer efficiency fault may cause substantial energy waste and hydrogen supply interruptions, with significant economic losses. Therefore, for health management in power and integrated energy systems, it is essential to weight different diagnostic errors according to their operational-economic impacts.

At the system-architecture level, Schrotenboer *et al.* developed a Green Hydrogen Energy System integrating wind generation, hydrogen storage, and electricity/hydrogen markets [4]. Zhao *et al.* established a comprehensive physical model for offshore wind–hydrogen integrated systems, conducted simulation with fault injection [5]. These works motivate a realistic system boundary for this study: fluctuating wind power upstream, electrolyzers and tanks midstream, and hydrogen users downstream.

Additionally, within the integrated power system, production, storage, and maintenance are inherently coupled. This motivates the adoption of a maintenance model considering production-batch relationships. The Economic Manufacturing Quantity (EMQ) model is a classical production–inventory optimization tool. EMQ quantifies the relationships among batch size, inventory level, and cost under finite production rate and stable demand. By modeling the wind–hydrogen–storage system as an EMQ-type production–inventory system and mapping energy/material-flow parameters to production–inventory variables, inventory holding cost and shortage cost can be naturally introduced. Moreover, preventive maintenance, corrective maintenance, and downtime can be unified within a "cycle cost" framework, enabling a consistent economic indicator for both fault diagnosis and maintenance decision-making.

The main contributions are summarized as follows:

• A maintenance-cost-driven explainable fault diagnosis network based on CNN–BiLSTM is developeds, enabling joint optimization of diagnostic accuracy and operating cost.

• A unified wind–hydrogen production–hydrogen storage system model is established and mapped to an EMQ production–inventory system.

• A diagnosis–maintenance cost model considering downtime-induced shortage is derived, yielding a unified economic metric for diagnosis and maintenance decisions.

• A simulation platform is built to validate the proposed method. Multi-class fault datasets are generated via fault injection.

2. The Wind–Hydrogen Production–Hydrogen Storage Integrated System

2.1. *System Architecture*

The considered integrated system consists of four major subsystems: a wind farm, a battery energy storage system, a water electrolysis hydrogen production system, and hydrogen storage with downstream hydrogen loads. The corresponding energy and material flow can be summarized as in Fig. 1.

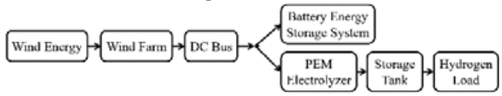

Fig. 1. Energy/material flow of integrated system.

In this framework, the wind farm converts stochastic wind energy into electricity with output power $P_{\text{wind}}(t)$. The battery storage smooths wind power fluctuations and outputs $P_{\text{bat}}(t)$. The PEM electrolyzer operates under input power $P_{\text{el}}(t)$ and converts electricity into hydrogen mass flow $\dot{m}_{H_2}(t)$. The hydrogen tank stores hydrogen inventory $I(t)$, and downstream hydrogen demand consumes hydrogen at rate $d(t)$, representing industrial hydrogen usage or hydrogen-to-power applications. Overall, the operational objective is to satisfy hydrogen demand while maximizing wind energy utilization and minimizing the long-term comprehensive cost of production, inventory, and maintenance.

2.2. *Component Physical Models*

To support fault injection and dataset construction, simplified physical models are adopted.

2.2.1. *Wind Farm Model*

For a single wind turbine, the aerodynamic power under wind speed $v_w(t)$ is:

$$P_{\text{aero}}(t) = \frac{1}{2}\rho A v_w^3(t) C_p(\lambda(t), \beta(t)), \quad (1)$$

where ρ is air density, A is swept area, λ is tip-speed ratio, β is pitch angle, and C_p is the power coefficient.

Wind turbines typically employ maximum power point tracking (MPPT) and pitch–torque coordinated control to keep output power smooth around the rated region. When sensor/actuator faults occur, the controller may misinterpret operating conditions, resulting in power loss or amplified fluctuations.

The mechanical–electromagnetic dynamics can be simplified as:

$$J\frac{d\omega_r}{dt} = T_{\text{aero}} - T_g^{\text{cmd}} - D\omega_r, \tag{2}$$

where ω_r is rotor angular speed and T_g^{cmd} is the generator torque command. Accounting for generator and converter losses yields the DC-side power used by downstream subsystems.

2.2.2. *Battery Energy Storage Model*

A first-order equivalent model is used. Let battery terminal voltage be V_{bat}, current I_{bat}, and state of charge SOC. Then:

$$V_{\text{bat}} = V_{\text{nom}} - R_{\text{int}} I_{\text{bat}},$$
$$\text{SOC}_{k+1} = \text{SOC}_k - \frac{P_{\text{bat}}(k)\Delta t}{E_{\text{cap}}}, \tag{3}$$

where R_{int} is internal resistance and E_{cap} is rated energy capacity. By coordinating the allocation between $P_{\text{bat}}(t)$ and $P_{\text{el}}(t)$, the battery mitigates wind-power fluctuations seen by the electrolyzer.

Battery faults such as capacity fade or resistance increase reduce the buffering ability against wind variability, indirectly degrading the effective hydrogen production rate.

2.2.3. *PEM Electrolyzer Model*

With electrical power as input and nominal efficiency η, the hydrogen production rate can be approximated as:

$$p = \frac{\eta P_{\text{el}}(t)}{E_{H_2}}, \tag{4}$$

where $E_{H_2}\,(\text{J}/\text{kg})$ is the theoretical electricity consumption per unit hydrogen production. PEM stack faults decrease η and thus reduce hydrogen output under the same input power.

2.2.4. *Hydrogen Storage and Demand Model*

Let hydrogen inventory in the tank be $I(t)(\text{kg})$ and downstream demand be $d(t)$. The mass balance is:

$$\frac{dI(t)}{dt} = \dot{m}_{H_2}(t) - d(t), \tag{5}$$

where the average demand rate d corresponds to industrial hydrogen use, hydrogen-to-power generation, etc. The tank capacity $I_{\max}^{\text{tank}}$ provides the inventory upper bound.

3. Production–Inventory and Maintenance Cost Model

3.1. *EMQ Formulation for the Energy System*

The EMQ model describes a continuous production–inventory system with stable demand and finite production rate. It quantifies how production batch size and inventory profiles affect total cost. In the studied system, the PEM electrolyzer produces hydrogen under wind support. Its equivalent hydrogen production rate is $p(\text{kg}/\text{h})$ (in Section 2.2.3), while the downstream average demand is $d(\text{kg}/\text{h})$, with $p > d$. For each production cycle, the planned production quantity is $Q\ (\text{kg})$, and the hydrogen inventory is $I(t)(\text{kg})$. Each start-up/shutdown or operating-point reconfiguration incurs a fixed setup cost S. Hydrogen holding cost is H per unit hydrogen per unit time, and shortage cost is h_s per unit unmet hydrogen, with $h_s > H$.

The typical EMQ inventory trajectory yields:

Production phase duration:

$$t_p = \frac{Q}{p}. \tag{6}$$

Cycle length:

$$T = \frac{Q}{d}. \tag{7}$$

Maximum inventory:

$$I_{\max} = Q\left(1 - \frac{d}{p}\right). \tag{8}$$

Average inventory:

$$\bar{I} = \frac{I_{\max}}{2} = \frac{Q}{2}\left(1 - \frac{d}{p}\right). \tag{9}$$

This EMQ provides a principled way to express the economic implications of production, inventory, and demand shortage, and later to integrate maintenance-induced downtime into the same cycle-cost framework.

3.2. *Production and Inventory Cost Modeling*

Hydrogen production and storage costs, particularly electricity cost, are non-negligible. Let electricity price be $c_e\left(¥/\mathrm{kWh}\right)$. The electricity cost per unit hydrogen is:

$$c_{\text{prod}} = c_e \frac{E_{H_2}}{\eta_0}, \tag{10}$$

where η_0 is the nominal electrolyzer efficiency.

With cycle production quantity Q, the cycle production cost is:

$$C_{\text{prod}} = c_{\text{prod}} Q. \tag{11}$$

The cycle inventory cost is:

$$C_{\text{inv}} = H\bar{I}T = H \cdot \frac{Q}{2}\left(1 - \frac{d}{p}\right) \cdot \frac{Q}{d}. \tag{12}$$

With setup cost S, the baseline EMQ cycle cost under normal operation is:

$$C_{\text{EMQ},base} = S + C_{\text{prod}} + C_{\text{inv}}. \tag{13}$$

The average cost rate is

$$G_{\text{EMQ}} = C_{\text{EMQ,base}} / T. \tag{14}$$

3.3 Downtime-Induced Shortage Cost

When the electrolyzer is shut down for maintenance, hydrogen demand is met by inventory until depletion. Define the inventory buffer time:

$$\tau_{\text{buf}} = \frac{I_{\text{max}}}{d}. \tag{15}$$

For a single downtime event lasting $\tau(\mathrm{h})$, if $\tau \le \tau_{\text{buf}}$, inventory can fully support demand and no shortage occurs. If $\tau > \tau_{\text{buf}}$, the shortage amount is approximately $d\left(\tau - \tau_{\text{buf}}\right)$.

Therefore, the shortage cost for one downtime event is:

$$C_{\text{shortage}}(\tau) = h_s \cdot \max\left(0, d\left(\tau - \tau_{\text{buf}}\right)\right). \tag{16}$$

This term explicitly quantifies the economic penalty of maintenance downtime beyond the system's inventory resilience, which is essential for differentiating the operational consequences of different diagnostic outcomes.

3.4 Maintenance Costs

For each fault type $i = 1, \ldots, 4$, two maintenance modes are considered:

(a) Preventive maintenance (PM) cost $C_{PM}(i)$: the total expense incurred when the fault is detected promptly and correctly, with a planned downtime duration $\tau_{PM}(i)$.

(b) Corrective maintenance (CM) cost $C_{CM}(i)$: the total expense incurred when the fault is missed or misdiagnosed and the system continues operating until failure, requiring major repair. CM leads to an unplanned downtime duration $\tau_{CM}(i)$.

In general, $C_{CM}(i) > C_{PM}(i)$ and, $\tau_{CM}(i) > \tau_{\text{buf}} > \tau_{PM}(i)$. as CM is both more expensive and more disruptive.

3.5 Scenario-Dependent Cycle Cost

Let i denote the true state and j the diagnosed state (0 indicates normal, 1-4 indicate four fault types). For each diagnostic scenario, the total cycle cost is defined as:

(a) True normal and diagnosed normal $(0 \to 0)$:

$$C_{00} = C_{\text{EMQ,base}}. \tag{17}$$

(b) True normal but false alarm as fault j $(0 \to j, j \ne 0)$:

$$C_{0j} = C_{\text{EMQ,base}} + C_{PM}(j) + C_{\text{shortage}}\left(\tau_{PM}(j)\right). \tag{18}$$

(c) Fault i correctly diagnosed $(i \to i)$:

$$C_{ii} = C_{\text{EMQ,base}} + C_{PM}(i) + C_{\text{shortage}}\left(\tau_{PM}(i)\right). \tag{19}$$

(d) Fault iii missed as normal $(i \to 0)$:

$$C_{i0} = C_{\text{EMQ,base}} + C_{CM}(i) + C_{\text{shortage}}\left(\tau_{CM}(i)\right). \tag{20}$$

(e) Fault i misclassified as another fault $j \ne 0, i$ $(i \to j)$:

$$C_{ij} = C_{\text{EMQ,base}} + \left[C_{PM}(j) + C_{\text{shortage}}\left(\tau_{PM}(j)\right)\right] + \left[C_{CM}(i) + C_{\text{shortage}}\left(\tau_{CM}(i)\right)\right]. \tag{21}$$

Cycle cost is normalized to an average cost rate:

$$G_{ij} = \frac{C_{ij}}{T}, \tag{22}$$

and the diagnosis–maintenance cost matrix is defined as:

$$C[i,j] := G_{ij}, \tag{23}$$

forming a 5×5 matrix. This matrix is the key interface between the EMQ-based economic model and the data-driven diagnostic model. It transparently encodes the economic severity of each type of diagnostic error and thus provides an interpretable, decision-oriented training signal.

4. Cost-Sensitive Fault Diagnosis Model

4.1 Problem Formulation

In the simulation of the wind–hydrogen–storage system, at each time step t_k, a feature vector is collected:

$$x_k = \left[v_w, \omega_r^{\text{meas}}, P^{\text{meas}}, \text{SOC}, V_{\text{bat}}, P_{\text{el}}, U_{\text{el}}, \dot{m}_{H_2} \right]_k, \tag{24}$$

where the features capture wind conditions, turbine measurements, power outputs, and hydrogen-production signals.

A sliding window of fixed length L forms the $n-$th sample:

$$\mathbf{X}^{(n)} = \left[x_{k_n}, x_{k_n+1}, \ldots, x_{k_n+L-1} \right] \in \mathbb{R}^{L\times d}, \tag{25}$$

with feature dimension d. The label is taken as the fault state at the window end:

$$y^{(n)} = y_{k_n+L-1} \in \{0,1,2,3,4\}, \tag{26}$$

Thus, the fault diagnosis task becomes learning a mapping $\mathcal{F}(\mathbf{X};\theta)$ that outputs the probability distribution over the five states $\hat{\boldsymbol{p}}$, and optimizes parameters θ by jointly considering diagnostic accuracy and EMQ-derived economic cost.

4.2 CNN–BiLSTM Architecture

To extract both local temporal patterns and longer-term dynamics, a CNN–BiLSTM network is adopted:

(a) 1D Convolution (CNN)

Multi-channel 1D convolution along the time axis extracts local change patterns:

$$h^{(1)} = \text{ReLU}\left(\text{Conv1D}\left(\mathbf{X}; W_c, b_c\right)\right), \tag{27}$$

The convolution kernels capture short-horizon trends, fluctuations, and local signatures indicative of incipient faults.

(b) Bidirectional LSTM (BiLSTM)

The convolutional feature sequence is fed into a BiLSTM:

$$h^{(2)} = \text{BiLSTM}\left(h^{(1)}\right), \tag{28}$$

The bidirectional structure leverages both past and future context within the window, modelling fault evolution.

(c) Fully Connected Layer and Output

A fully connected layer produces logits, and softmax yields state probabilities:

$$z = W_o h^{(2)} + b_o, \hat{p}_j = \frac{\exp(z_j)}{\sum_{l=0}^{4} \exp(z_l)}, j = 0,\ldots,4, \tag{29}$$

where the output $\hat{p}_j = \left[\hat{p}_0, \ldots, \hat{p}_4\right]$ is used for classification and computing expected economic loss.

4.3 EMQ-Based Expected Cost

Given the cost matrix G_{ij} derived in Section 3, for a sample with label y, the expected cost rate in the current cycle is approximated as:

$$\mathbb{E}\left[G | y, \hat{\boldsymbol{p}}\right] = \sum_{j=0}^{4} C\left[y, j\right] \hat{p}_j, \tag{30}$$

This term represents the EMQ-based economic indicator of the diagnostic decision.

4.4 Cost-Sensitive Training Strategy

Standard multi-class classification often uses cross-entropy loss:

$$\mathcal{L}_{\text{CE}}\left(y, \hat{\boldsymbol{p}}\right) = -\log \hat{p}_y, \tag{31}$$

which maximizes the probability of the true class but treats all misclassifications uniformly.

To incorporate EMQ cost, a cost-sensitive loss is defined:

$$\mathcal{L}\left(y, \hat{\boldsymbol{p}}\right) = \mathcal{L}_{\text{CE}}\left(y, \hat{\boldsymbol{p}}\right) + \lambda \sum_{j=0}^{4} C\left[y, j\right] \hat{p}_j, \tag{32}$$

where weight $\lambda > 0$ is tuned via cross-validation to reflect the desired trade-off between diagnostic performance and operational cost. First term balances accuracy and second term balances economic optimality.

During training, the loss is optimized via backpropagation and gradient-based methods.

5. Simulation Platform Construction

5.1 Simulation Scenario and Time Settings

To validate the proposed approach, a wind–battery–PEM electrolyzer integrated simulation platform is established. The total simulation duration is T_{sim} with time step Δt. Wind speed exhibits both medium/long-term trends and short-term randomness. The system runs through multiple operating cycles, each containing normal segments and fault segments.

5.2 Fault Types and Injection Methods

Four representative faults (plus a normal state) are considered:

Class 0 (ID_0): Normal, all subsystem parameters remain nominal.

Class 1 (ID_1): Turbine sensor fault, gain bias injected into rotor speed measurement:

$$\omega_r^{\text{meas}} = k_\omega \omega_r + n, k_\omega > 1, \tag{33}$$

where typical values $k_\omega = 1.2, n$ is Gaussian noise. This fault affects turbine output through the MPPT control loop.

Class 2 (ID_2): Turbine actuator fault, bias injected into generator torque command:

$$T_g^{\text{cmd}} = T_g^{\text{ref}} + \alpha_T T_g^{\text{rated}}, \tag{34}$$

which leading to derating or overload behaviour.

Class 3 (ID_3): Battery fault, capacity reduction and resistance increase:

$$E_{\text{cap}}^{\text{fault}} = \alpha_{\text{cap}} E_{\text{cap}}, R_{\text{int}}^{\text{fault}} = \beta_R R_{\text{int}}, \tag{35}$$

Class 4 (ID_4): Electrolyzer fault, stack efficiency drop:

$$\eta_{\text{fault}} = \gamma_\eta \eta_0, \gamma_\eta < 1, \tag{36}$$

which causing a significant hydrogen production reduction under the same input power.

Faults are injected according to a predefined timeline, e.g., 0–600 s normal, 600–900 s Class 1, 900–1200 s Class 2, 1200–1500 s Class 3, 1500–1800 s Class 4, then returning to normal. This schedule determines the ground-truth label y_k at each time step.

5.3 Dataset Split and Evaluation Metrics

The generated dataset is randomly split into training, validation, and test sets. To evaluate both diagnostic performance and economic effectiveness, three metrics are used: overall classification accuracy, macro-averaged F1 score, and EMQ-based average cost. This combination reflects multi-class recognition performance under class overlap/imbalance and the downstream maintenance-planning implications of diagnostic decisions.

6. Results and Discussion

6.1 Experimental Setup

This section compares a CNN–BiLSTM model trained with conventional cross-entropy (CE model) and the proposed cost-sensitive CNN–BiLSTM (Proposed model).

Under the same network architecture and training settings, two objectives are evaluated: CE-only loss versus the proposed cost-sensitive loss. Hyperparameters are referenced as Table 1.

Table 1. Hyperparameter in the experiments.

Energy-system parameters			
$P_{\text{el}}(t_0)$	η_0	c_e	E_{H_2}
1000(kW)	0.7	0.4(￥/kWh)	50(kWh/kg)
EMQ and maintenance parameters			
S	d	h_s	H
20000(￥)	10(kg/h)	200(￥/kg)	0.02(￥/kg*h)
C_{PM1}	C_{PM2}	C_{PM3}	C_{PM4}
15000(￥)	25000(￥)	35000(￥)	60000(￥)
τ_{PM1}	τ_{PM2}	τ_{PM3}	τ_{PM4}
5(h)	8(h)	12(h)	16(h)
C_{CM1}	C_{CM2}	C_{CM3}	C_{CM4}
40000(￥)	90000(￥)	180000(￥)	320000(￥)
τ_{CM1}	τ_{CM2}	τ_{CM3}	τ_{CM4}
24(h)	72(h)	120(h)	300(h)

6.2 Class Separability and Visualization

In the simulated dataset, Fault-3 and the normal state are the most difficult to distinguish. Pair 0-3 cross-classification rates reach 0.351 and 0.462, respectively. PCA visualization based on window-mean features further confirms local overlap among classes, as shown in Fig. 2., where misclassified samples in preliminary experiments are also marked.

Fig. 2. PCA visualization showing inter-class overlap and misclassified samples.

6.3 Diagnostic Performance and Economic Outcomes

With identical architecture and data splits, the cost-sensitive model achieves slightly improved accuracy and macro-F1 compared with the CE-only model, while reducing the long-term average operating cost under the EMQ criterion by approximately 7.2%. This indicates that introducing the cost term does not degrade classification performance, but can substantially improve maintenance-related economic outcomes. The reason is that cost-sensitive training biases the decision boundary to avoid high-cost mis-diagnosis, even if that slightly increases the probability of low-cost errors in marginal cases.

Table 2. Comparison of Model Results.

	Accuracy	F1	G-mean	Costs
CE model	0.9185	0.9160	0.9099	363.4136
Proposed model	0.9942	0.9942	0.9942	337.3474

Confusion-matrix analysis shows that the CE-only model has lower recall for the normal state and Fault-3; in particular, Fault-3 is more frequently misclassified as normal (about 25%). The cost-sensitive model significantly reduces this high-cost error: the recall of Fault-3 increases from 0.7422 to 0.9943, demonstrating the advantage of cost-aware learning in preventing economically severe misdiagnoses.

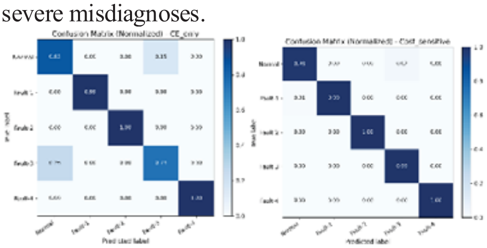

Fig. 3. Confusion-matrix analysis.

Overall, these results validate the effectiveness of the proposed cost-sensitive training strategy in practical settings where diagnostic accuracy must be balanced against operational and maintenance economics.

7. Conclusions and Future Work

This paper proposes an EMQ-based cost-sensitive fault diagnosis method for wind–hydrogen production–hydrogen storage integrated energy systems.

A unified wind model is established and abstracted into a production–inventory system. By integrating preventive and corrective maintenance, a cycle-cost model that accounts for downtime-induced shortage and maintenance expenditures is derived. The resulting diagnosis–maintenance cost matrix is embedded into the training objective of a CNN–BiLSTM diagnostic network, enabling joint optimization of fault recognition accuracy and operating cost.

Future work will extend the framework by considering more fault and degradation modes, incorporating electricity price volatility, and co-optimizing wind farm dispatch parameters together with health management decisions to improve system-level economic performance and resilience.

References

Zhang, Jianping, and Jie Liu. (2026). Deconfounding Enhanced Image-Based Knowledge Distillation for Fault Diagnosis with an Application in Manufacturing Process. *Engineering Applications of Artificial Intelligence* 163 (January): 112907.

Zheng, Shuwen, Kai Pan, Jie Liu, and Yunxia Chen. (2024). Empirical Study on Fine-Tuning Pre-Trained Large Language Models for Fault Diagnosis of Complex Systems. *Reliability Engineering & System Safety* 252 (December): 110382.

Zheng, Shuwen, Chong Wang, Enrico Zio, and Jie Liu. (2024). Fault Detection in Complex Mechatronic Systems by a Hierarchical Graph Convolution Attention Network Based on Causal Paths. *Reliability Engineering & System Safety* 243 (March): 109872.

Schrottenboer, Albert H., Arjen A.T. Veenstra, Michiel A.J. uit het Broek, and Evrim Ursavas. (2024). A Green Hydrogen Energy System: Optimal Control Strategies for Integrated Hydrogen Storage and Power Generation with Wind Energy. *Applied Energy* 325: 1–15.

Zhao, Tianxiang, Shucai Feng, Yilai Zhou, Zhuang Kang, and Jichuan Kang. (2024). Data-Driven Fault Detection Framework for Offshore Wind-Hydrogen Systems. *International Journal of Hydrogen Energy* 70: 325–340.